TISSUE ENGINEERING: Part C
Volume 21, Number 12, 2015
© Mary Ann Liebert, Inc.
DOI: 10.1089/ten.tec.2015.0135

termis
Tissue Engineering
& Regenerative Medicine
International Society

METHODS ARTICLE

Three-Dimensional Neural Spheroid Culture: An *In Vitro* Model for Cortical Studies

Yu-Ting L. Dingle, PhD,[1,2,*] Molly E. Boutin, BS,[1,2,*] Anda M. Chirila, PhD,[1] Liane L. Livi, MS,[1] Nicholas R. Labriola, BS,[1,2] Lorin M. Jakubek, PhD,[1,2] Jeffrey R. Morgan, PhD,[1–3] Eric M. Darling, PhD,[1–4] Julie A. Kauer, PhD,[1,5,6] and Diane Hoffman-Kim, PhD[1–3,6]

There is a high demand for *in vitro* models of the central nervous system (CNS) to study neurological disorders, injuries, toxicity, and drug efficacy. Three-dimensional (3D) *in vitro* models can bridge the gap between traditional two-dimensional culture and animal models because they present an *in vivo*-like microenvironment in a tailorable experimental platform. Within the expanding variety of sophisticated 3D cultures, scaffold-free, self-assembled spheroid culture avoids the introduction of foreign materials and preserves the native cell populations and extracellular matrix types. In this study, we generated 3D spheroids with primary postnatal rat cortical cells using an accessible, size-controlled, reproducible, and cost-effective method. Neurons and glia formed laminin-containing 3D networks within the spheroids. The neurons were electrically active and formed circuitry through both excitatory and inhibitory synapses. The mechanical properties of the spheroids were in the range of brain tissue. These *in vivo*-like features of 3D cortical spheroids provide the potential for relevant and translatable investigations of the CNS *in vitro*.

Introduction

Disease and injury in the central nervous system (CNS) have tremendous impacts on quality of life, and there is a high demand for models to study CNS pathologies and therapeutic strategies. Neurons and glial cells in the brain form a complex three-dimensional (3D), intertwined system and, therefore, engineering the microenvironment for *in vitro* investigations presents many inherent challenges.[1] Microenvironmental cues, such as cellular, biochemical, mechanical, and topographical cues, can influence cell behaviors, including viability, proliferation, differentiation, migration, and protein and gene expressions.[2–6] Notably, many native microenvironmental cues are lost in traditional two-dimensional (2D) cultures, in which cells spread on substrates that are often several orders of magnitudes stiffer than brain tissue and lack the brain's extracellular matrix (ECM) organization.[7] Cells in 2D are forced to adapt a planar morphology and can form intercellular connections only in the lateral direction. These deficiencies have led to the development of 3D *in vitro* models of the nervous system.

Three-dimensional *in vitro* neural models have exciting potential to bridge the gap between traditional 2D cultures and *in vivo* models.[1,8] For example, 3D culture of human induced pluripotent stem cells has enabled the study of microcephaly,[9] and the hallmarks of Alzheimer's disease, amyloid-β plaques, and neurofibrillary tangles, have been more effectively modeled in 3D cultures than in 2D.[10] Historically, 3D neural cultures were developed using scaffolds,[3,11–14] and complex cell compartmentalization and organization have been achieved through scaffold design.[15–17] Recently, neural cells have been cultured through self-assembly into spheroid structures in which they can produce their own matrix;[18,19] these spheroids have been suggested to approximate *in vivo*-like cell behavior better than scaffold-based cultures.[20,21]

Several studies of the nervous system function or disease have incorporated high levels of technological requirements in their cell cultures.[9,16,17,22,23] Combinations of advances, including multicomponent scaffold design, progenitor cells, and long-term culture, have given rise to sophisticated *in vitro* models of the nervous system. However, complex neural cultures may be unattainable to many labs due to the

[1]Department of Molecular Pharmacology, Physiology, and Biotechnology, Brown University, Providence, Rhode Island.
[2]Center for Biomedical Engineering, Brown University, Providence, Rhode Island.
[3]School of Engineering, Brown University, Providence, Rhode Island.
Departments of [4]Orthopedics and [5]Neuroscience, Brown University, Providence, Rhode Island.
[6]Brown Institute for Brain Science, Brown University, Providence, Rhode Island.
*Equal contributions to this work.

resources and expertise needed to assemble and maintain them. In this study we have characterized a relatively simple 3D neural culture approach that provides access to laboratory groups that wish to address the myriad of interesting questions in neurobiology and neuroengineering.

This reproducible method to generate 3D neural spheroids utilizes culture materials that are commercially available, or alternatively can be fabricated by a laboratory through standard biomaterial techniques. This approach requires no progenitor or embryonic cell isolation; only postnatal cultures are needed. We show that in the relatively short time frame of 2 weeks, the 3D postnatal cortical neural spheroid contains neurons, glia, and cell-synthesized matrix, is mechanically similar to *in vivo* cortex, and is electrically active. This approach can provide relatively large numbers of 3D microtissues for the study of CNS function, disease, and therapeutics.

Materials and Methods

Cell isolation and culture

Primary cortical tissues were isolated from postnatal day 1–2 CD rats (Charles River), and primary rat hippocampus tissues (embryonic day 18) were purchased from BrainBits, LLC. Cell isolation protocol was modified from BrainBits. The following buffer solutions and media were used: Hibernate A buffer solution—Hibernate A (BrainBits, LLC) supplemented with 1× B27 supplement (Invitrogen) and 0.5 mM GlutaMAX (Invitrogen); Papain solution –2 mg/mL papain dissolved in Hibernate A without Calcium (BrainBits, LLC); Neurobasal A/B27 medium—Neurobasal A medium (Invitrogen) supplemented with 1× B27, 0.5 mM GlutaMAX, and 1× Penicillin–Streptomycin (Invitrogen). Briefly, the tissues were cut into small pieces and placed in papain solution for 30 min at 30°C. Papain solution was removed, and the tissues were triturated with fire-polished Pasteur pipettes 20 times in Hibernate A buffer solution. The cell solution was centrifuged at 150 *g* for 5 min, and the supernatant was removed. The cell pellet was resuspended in Neurobasal A/B27 medium, and debris was removed by passing the solution through a 40 μm cell strainer. The cell solution was washed once more by centrifuging at 150 *g* for 5 min, resuspending in Neurobasal A/B27 medium, and filtering with a cell strainer. Cell viability at the time of isolation was determined by a Trypan Blue Exclusion Assay (Invitrogen). Cortical cells were seeded at densities of 1000, 2000, 4000, and 8000 (1k, 2k, 4k, 8k) cells/spheroid (see Three-dimensional self-assembled cortical spheroid fabrication). All results are from at least three independent experiments. Hippocampal cells were seeded at densities of 125, 1000, and 3300 cells/spheroid.

Three-dimensional self-assembled cortical spheroid fabrication

Molten 2% agarose (Invitrogen) solution was poured onto the spheroid micromold with 400-μm diameter round pegs (#24–96-Small, MicroTissues, Inc.) to obtain agarose hydrogels with round-bottomed recesses, termed microwells. Agarose gels were equilibrated in a culture medium with three medium exchanges over a 48-h period. Cell solution containing the appropriate number of cells was centrifuged and resuspended in Neurobasal A/B27 medium. Medium was aspirated from the gels, and the cell solution (75 μL/gel) was seeded in the agarose gels. Cells were allowed to settle into the microwells for 30 min, and 1 mL Neurobasal A/B27 medium was added. Cell medium was exchanged 48 h after seeding and subsequently every 3–4 days.

Whole spheroid immunostaining and optical clearing

Whole spheroid immunostaining and Clear^{T2} clearing protocols were adopted.[24,25] Briefly, spheroids were fixed in 4% v/v paraformaldehyde and 8% w/v sucrose in phosphate-buffered saline (PBS) overnight, followed by three 1-h PBS washes. All of the following steps were performed on a shaker at room temperature. The following antibodies were used: mouse anti-β-III-tubulin (Covance MMS-435P, 1:50), rabbit anti-glial fibrillary acidic protein (GFAP, DAKO Z0334, 1:200), rabbit anti-laminin (BTI BT594, 1:100), mouse anti-nestin (Millipore MAB353, 1:200), mouse anti-CD11b (Millipore CBL1512, 1:25), mouse anti-O1 (Millipore MAB344, 1:50), Cy3 goat anti-mouse (Jackson 115-165-068, 1:500), and Alexa488 goat anti-rabbit (Jackson 115-545-146, 1:500). Spheroids were permeabilized and blocked with 1% Triton X-100 (TX), 10% normal goat serum (NGS), and 4% bovine serum albumin (BSA) in PBS (B-PBT) for 2 h, and subsequently incubated in primary antibodies diluted in B-PBT overnight. Spheroids underwent two 2-h washes with 0.2% TX in PBS (PBT), followed by one 2-h B-PBT wash. Spheroids were incubated with secondary antibodies in B-PBT overnight. Spheroids underwent two 2-h PBT washes and incubated in 1 μg/mL 4′,6-diamidino-2-phenylindole (DAPI) in PBT for 1 h and returned to PBS.

Clear^{T2} 20% and 40% w/v polyethylene glycol (PEG) solutions were made in water and 50% v/v formamide (Sigma) solution was made in PBS. The following incubation steps were used: (1) 25% formamide/10% PEG for 10 min, (2) 50% formamide/20% PEG for 5 min, and (3) 50% formamide/20% PEG for 60 min. Spheroids were kept in a final clearing solution and transferred to glass-bottomed confocal dishes for imaging.

Spheroid cryosectioning and immunostaining

Spheroid embedding, cryosectioning, and immunostaining protocols were adapted.[24,25] Briefly, spheroids were fixed and washed as described (see Three-dimensional self-assembled cortical spheroid fabrication) and subjected to a sucrose gradient of 15% and 30% w/v sucrose in PBS, for 3 h per step. Whole agarose gels containing spheroids were embedded in O.C.T. Compound (Tissue-Tek #4583) and stored at –80°C. Sections, 8 μm thick, were cut using a Leica CM3050 S Cryostat and placed on SuperFrost Plus slides (Fisher Scientific).

Spheroid sections were brought to room temperature, fixed for 10 min in 4% v/v paraformaldehyde, and washed twice with PBS. Cells were then permeabilized with 0.1% TX in PBS for 15 min and washed twice with PBS. Samples were blocked with a solution of 2% BSA, 10% NGS, and 0.1% TX for 1 h. Sections were then incubated overnight at 4°C in a humidified chamber with mouse anti-NeuN (Millipore MAB377 1:50) in PBS. Following primary antibody incubation, sections were washed twice for 30 min each in PBS, followed by a 30 min wash with 0.1% TX in PBS. Secondary antibody, Cy3 goat anti-mouse, was diluted in PBS and sections were incubated with secondary antibody solution for 1h at room temperature. Subsequently, sections were washed for 10 min with 0.1% TX, and twice for 5 min each with PBS.

Sections were incubated in DAPI solution for 7 min, followed by two 5 min PBS washes. Sections were then mounted with Fluoromount-G (SouthernBiotech 0100-01).

Imaging and image analysis

For spheroid top-view diameter measurements, phase contrast images were taken by a Nikon CoolPix 995 camera connected to a Nikon TS200 microscope with a 10× objective. Spheroid diameters were measured in Fiji software. Cell densities at 1 day *in vitro* (DIV) were calculated by dividing the number of cells seeded by the spheroid volumes at 1 DIV. Three independent experiments were performed. For each density and time point, 12–36 spheroids were measured.

For immunofluorescence, confocal imaging of whole spheroids and spheroid sections was performed on a Zeiss LSM 510 Meta Confocal Laser Scanning Microscope built on an Axiovert 200M inverted microscope with ZEN 2009 software. 10×, 20×, and 40× objectives were used. For Z-stack images, laser power was kept constant, and gain was adjusted using the AutoZ Brightness Correction function. Three-dimensional projections were reconstructed in ZEN.

Cell densities at 14 and 21 DIV were calculated by dividing the number of cells in a confocal slice by the slice volume (Equation 1). DAPI-stained nuclei were automatically counted in Fiji software using Watershed separation algorithm and particle analysis tool. Cell number was found by normalizing DAPI-stained nuclei counts (N) to take into account the potential for a nucleus (diameter, $d = 10.23\,\mu m$) to cross multiple slices (thickness, $t = 2.01\,\mu m$). Volume was calculated by measuring the spheroid diameter (D) within the confocal slice ($t = 2.01\,\mu m$).

$$\text{Cell density (cells/mm}^3) = \frac{N * (t/d)}{\pi * (D/2)^2 * t} = 124.46 * \frac{N}{D^2} \quad (1)$$

To obtain the percentage of mature neurons in 21 DIV 8k spheroids, 10× confocal images of central region spheroid sections were acquired. Quantification was performed manually in Fiji software using the Cell Counter plugin. DAPI-stained nuclei were manually counted, excluding nuclei with pyknotic appearances. The number of NeuN+ nuclei were counted and divided by total nuclei counts. All results were from three independent experiments, 20 sections per experiment.

Electrophysiology

Cortical spheroids were transferred from the hydrogels and immobilized by allowing the bottom of the spheroids to adhere onto poly-D-lysine (50 μg/mL)-coated coverslips for 2 days before clamp recordings. Spheroids were perfused at ~1 mL/min at room temperature with oxygenated artificial cerebrospinal fluid (aCSF) containing 2.5 mM $CaCl_2$, 1 mM NaH_2PO_4, 119 mM NaCl, 2.5 mM KCl, 1.3 mM $MgSO_4$, 26 mM $NaHCO_3$, 25 mM dextrose, and 1.3 mM Na ascorbate. Whole-cell voltage clamp recordings at −70 mV were made from neurons near the surface (<3 cell layers) on the spheroid using patch pipettes filled with a KCl-based internal solution containing 125 mM KCl, 2.8 mM NaCl, 2 mM $MgCl_2$, 2 mM ATP-Mg^{2+}, 0.3 mM GTP-Na^+, 0.6 mM EGTA, and 10 mM HEPES. Current clamp recordings were made with no added holding current. For spontaneous excitatory postsynaptic currents (sEPSCs), aCSF contained bicuculline (10 μM) and strychnine (10 μM) to block $GABA_A$ and glycine receptors; for spontaneous inhibitory postsynaptic currents (sIPSCs), 6,7-dinitroquinoxaline-2,3-dione (DNQX; 10 μM) was added to block AMPA receptors.

Mechanical characterization

Mechanical properties were tested with an MFP-3D-BIO atomic force microscope (AFM, Asylum Research) connected to a Nikon Eclipse Ti-U epifluorescence microscope. Spheroids were harvested and immobilized (see Electrophysiology). Neonatal cortex was manually sectioned and immobilized on a glass coverslip with 2% low-melt SeaPrep Agarose in water (Cambrex). A $40 \times 40\,\mu m^2$ measurement area was selected on the top surface of each spheroid, and 4×4 measurement points were evenly placed in the area. Indentation curves were measured using a spherically tipped cantilever (5 μm diameter, average $k \sim 0.027$ N/m, Novascan Technologies, Inc.) with an approach velocity of 10 μm/s, and force trigger of 1 nN, following previously established procedures.[26] Between 11 and 19 spheroids were tested at each time point from 2–3 independent experiments. Average indentation depth was >2 μm. Elastic modulus was calculated from force (F) versus indentation curves (δ) using a modified Hertz model (Equation 2) previously described.[27–29] In the equation, R is the effective radius of the cantilever tip, and v is the Poisson's ratio, assumed to be 0.5 for incompressible materials. Outliers, defined as >10 Pa and <2.5× standard deviation, were removed. Geometric means of the moduli were calculated. One-way ANOVA with *post hoc* multiple comparisons using Bonferroni test was used to perform statistical analysis.

$$F(\delta) = \frac{4R^{1/2}E_{elastic}}{3(1-\upsilon^2)}\delta^{3/2} \quad (2)$$

Results

Cortical cells self-assembled into 3D spheroids

Monodispersed cortical cells were seeded in the micromolded hydrogels at seeding densities of 1k, 2k, 4k, and 8k per microwell. The hydrogel microwells facilitated the assembly of spheroids within 24 h. Spheroid diameters at 1 DIV ranged from 100–230 μm, with size dependent on the initial seeding density (Fig. 1a, b). Cell density in 1 DIV spheroids was estimated to be 2×10^6 cells/mm^3, independent of initial seeding density. Spheroid diameter increased from 1 DIV to 7 DIV, and between 7 and 21 DIV, less diameter growth was observed (Fig. 1b). Spheroid diameters were reproducible within and across experiments (Supplementary Fig. S1; Supplementary Data are available online at www.liebertpub.com/tec). Cell densities in 14 and 21 DIV spheroids (seeded at 8k cells/spheroid) were estimated to be $2–4 \times 10^5$ cells/mm^3. DAPI staining of central cryosections showed that spheroids contained healthy cells that were closely packed at 1 DIV (Fig. 1c). At 21 DIV, spheroids contained cells that were more spread and included healthy cells as well as centrally located cells with fragmented nuclei (Fig. 1c).

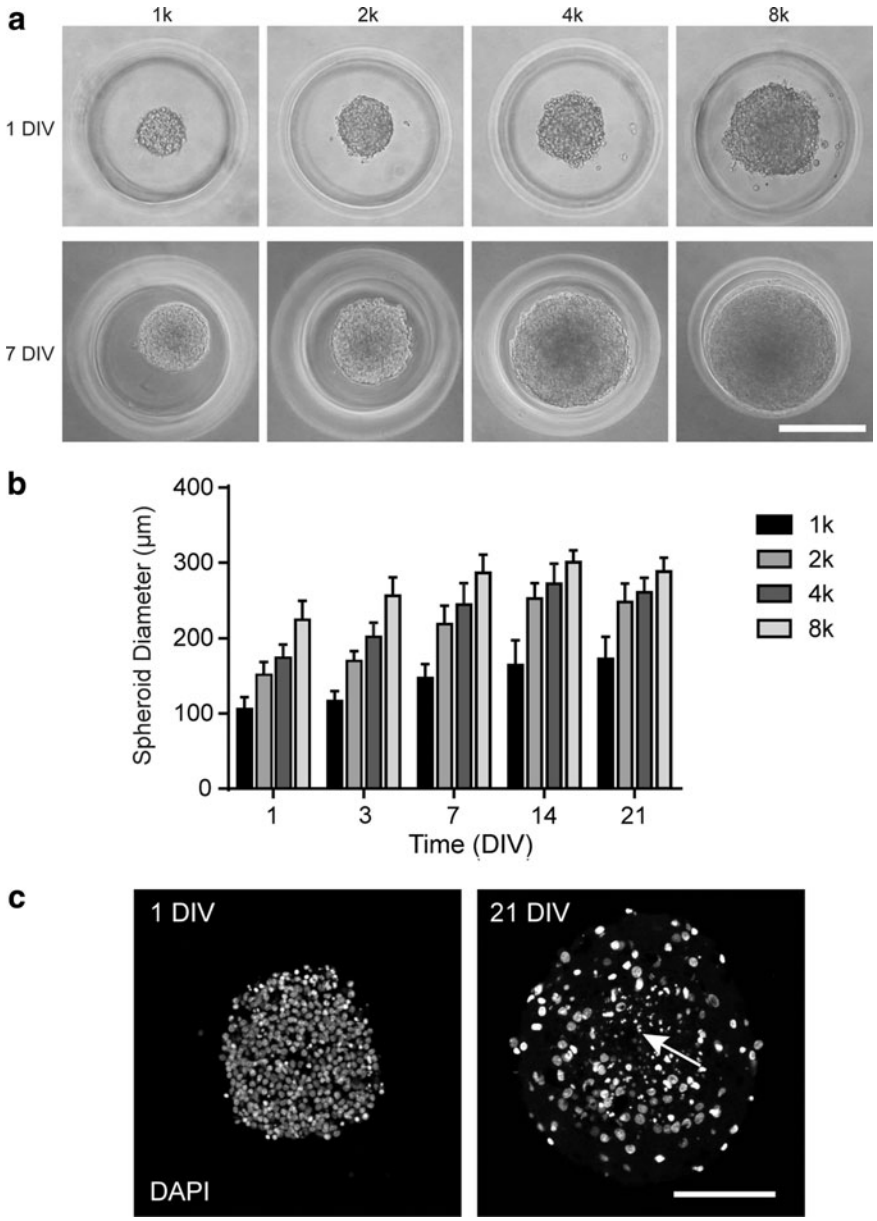

FIG. 1. Size-controlled 3D cortical spheroids. Monodispersed cortical cells self-assembled into spheroids in the micromolded hydrogels and contained viable cells for 21 days. **(a)** Phase contrast images of cortical spheroids at 1 DIV and 7 DIV with initial seeding densities of 1k, 2k, 4k, and 8k cells/spheroid. **(b)** Graph of spheroid diameter over time. Spheroid sizes initially increased, then plateaued. Each bar represents 70–86 spheroids that were measured from three independent experiments. Mean ± SD. **(c)** Confocal images of spheroid central cryosections stained with DAPI at 1 DIV and 21 DIV. Cells were initially closely packed and became more spread over time. *Arrow*, fragmented nucleus. Scale bars: **(a)** 200 μm and **(c)** 100 μm. 3D, three-dimensional; DAPI, 4′,6-diamidino-2-phenylindole; DIV, day *in vitro*.

Neurons and glia formed complex 3D structures in the spheroids

Neurons and glia were present in the cortical spheroids and included astrocytes, oligodendrocytes, and microglia, as well as neural stem/progenitor cells (Fig. 2). At 1 DIV, 8k spheroids exhibited globular patterns of β-III-tubulin neuronal and O1 oligodendrocyte staining, with short extensions from GFAP+ astrocytes, nestin+ neural stem/progenitor cells, and CD11b+ microglia. Cells were highly packed at this initial stage. From 1 to 7 DIV, the distance between nuclei increased (Fig. 2, DAPI). Neurites and longer cellular extensions were visible by 7 DIV. From 7 to 21 DIV, neurites elongated, formed bundles, and formed a complex network, and other cells continued extending processes. Neurites and cellular processes extended in all x, y, z directions (Supplementary Fig. S2 and Supplementary Movie S1). Spheroid cell composition at 21 DIV was reproducible and was split almost evenly between NeuN+ neurons (46 ± 7%) and other cells, including NeuN− immature neurons and non-neuronal cells (54%) (Supplementary Fig. S3). Laminin expression was detected in spheroids at all time points, and was generally diffuse, with some areas of localized brighter staining (Fig. 2, laminin).

Neurons in spheroids were electrically active and formed synaptic connections

Whole cell patch-clamp recordings were used to characterize the neurons' electrophysiological properties, including resting membrane potential, evoked action potentials, spontaneous action potentials, and spontaneous postsynaptic currents (PSCs). Average resting membrane potential for 7 DIV spheroids was −42.7 ± 6.8 mV ($n = 8$ cells). In response to a current injection, neurons in 7 DIV spheroids usually failed to fire an action potential or fired rapidly, failing broad small action potentials (Fig. 3a). Although sEPSCs (Fig. 3b, +bicuculline +strychnine panel) and sIPSCs (Fig. 3c, +DNQX

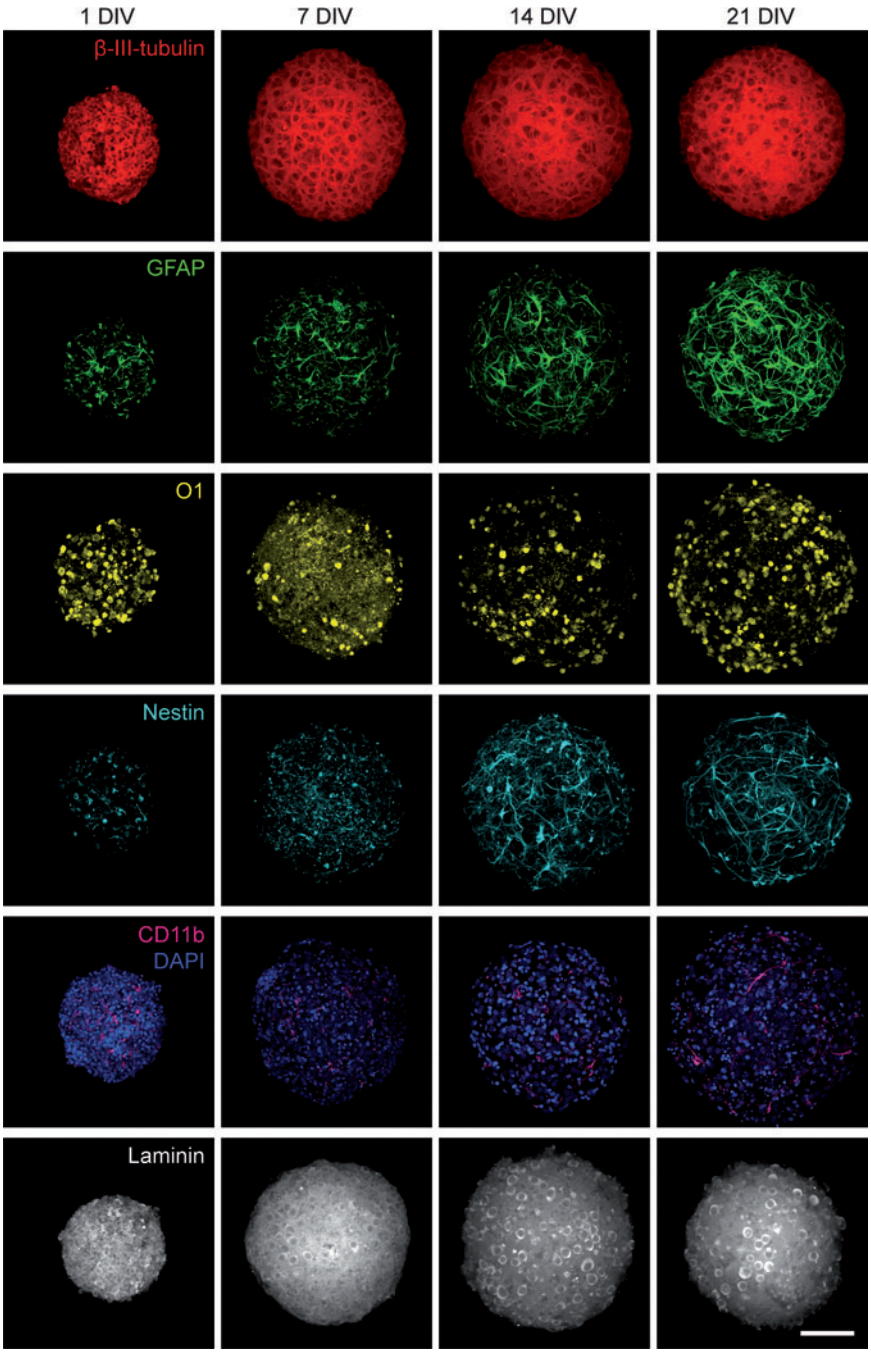

FIG. 2. Cortical spheroids contained CNS cell types, and cells formed laminin-containing 3D networks. Confocal projections of 1, 7, 14, and 21 DIV 8k spheroids revealed the presence of CNS cell types in the cortical spheroids, including neurons (β-III-tubulin, *red*), astrocytes (GFAP, *green*), oligodendrocytes (O1, *yellow*), neural stem/progenitor cells (nestin, *cyan*), and microglia (CD11b, *magenta*). Nuclei were counterstained with DAPI (*blue*). Cell processes formed 3D networks within the cortical spheroids. Confocal projections showed laminin expression (*gray*) in the cortical spheroids. Scale bar: 100 μm. CNS, central nervous system. GFAP, glial fibrillary acidic protein. Color images available online at www.liebertpub.com/tec

panel) could be detected, they were of low frequency and low amplitude.

In 14 DIV spheroids, average resting membrane potential was -56 ± 5.7 mV ($n = 7$). Neurons fired both evoked action potentials upon current injection (Fig. 4a) and spontaneous action potentials (Fig. 4b), suggesting that the neurons in 14 DIV spheroids were more mature than in 7 DIV spheroids. Among the neurons recorded, we detected repetitive spike, single spike, and delayed evoked action potential firing patterns (repetitive firing is illustrated in Fig. 4a). sEPSCs (Fig. 4c, +bicuculline +strychnine panel) and sIPSCs (Fig. 4d, +DNQX panel) of both large and small amplitudes were isolated using AMPA and $GABA_A$ receptor antagonists, respectively. Inhibiting sodium channels with tetradotoxin (TTX) blocks action potential-triggered PSCs. Quantal events (miniature PSCs) caused by the spontaneous fusion of neurotransmitter vesicles with the presynaptic membrane were detectable under these conditions (Fig. 4d, +TTX panel). These results demonstrate that both glutamatergic and GABAergic neurons are present in the spheroids, and the spontaneous PSCs demonstrate that both types of neurons make active synaptic connections onto the recorded neuron. Similarly to 14 DIV spheroids, evoked and spontaneous action potentials, as well as sEPSCs and sIPSCs, were detected in 21 DIV spheroids (Supplementary Fig. S4), showing that the neurons remained active. The average resting membrane potential for 21 DIV spheroids was -59 ± 5.2 mV ($n = 8$).

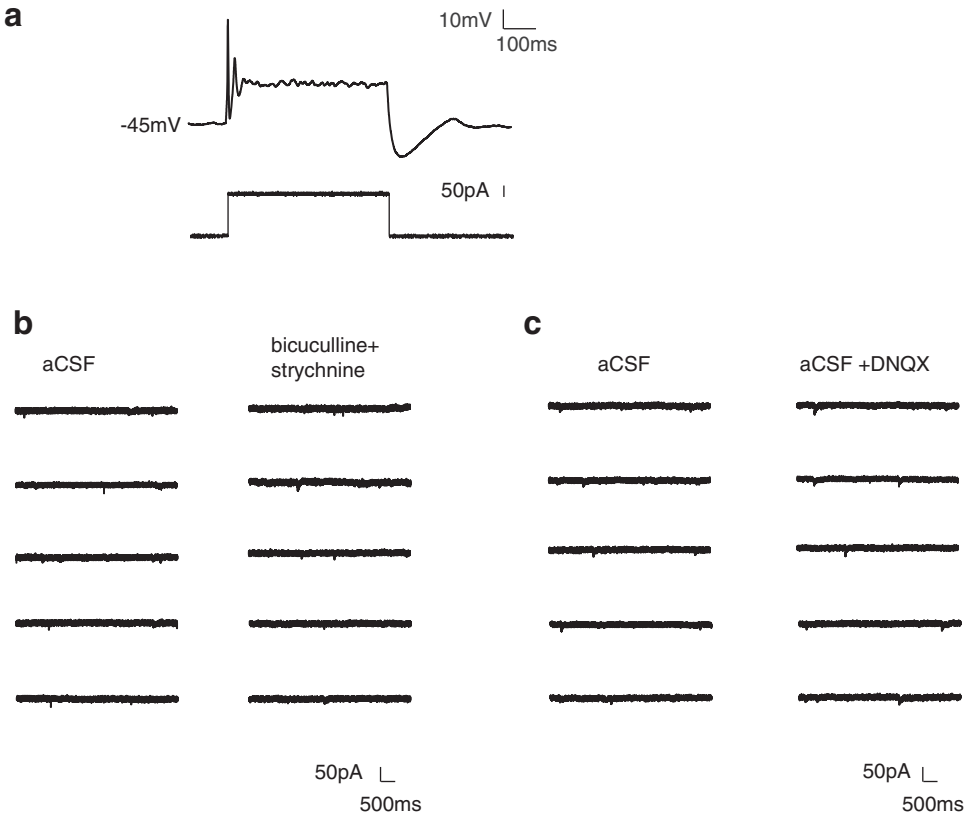

FIG. 3. Seven DIV spheroids contained neurons with immature properties. Neurons in 7 DIV 8k spheroids either failed to fire an action potential upon current injection or fired low amplitude, failing action potentials. **(a)** Example of a recorded neuron responding to somatic current injections by firing short, rapidly failing action potentials (current clamp recording). *Lower panel*: current injection protocol. **(b)** Example traces of spontaneous synaptic activity (voltage clamp recording holding the neuron at −70 mV). *Left panel*: spontaneous PSCs recorded in aCSF. *Right panel*: sEPSCs were isolated with $GABA_A$ receptor antagonist bicuculline and the glycine receptor antagonist strychnine. **(c)** *Left panel*: traces of spontaneous PSCs recorded in aCSF. *Right panel*: sIPSCs were isolated with the AMPA receptor antagonist DNQX. aCSF, artificial cerebrospinal fluid; DNQX, 6,7-dinitroquinoxaline-2,3-dione; PSCs, postsynaptic currents; sEPSCs, spontaneous excitatory postsynaptic currents; sIPSCs, spontaneous inhibitory postsynaptic currents.

Cortical spheroids had similar elastic moduli to cortical tissue

Elastic moduli of spheroids at 1, 7, 14, and 21 DIV and neonatal rat (P0-2) cortex tissues were assessed using AFM. As shown in Figure 5, there was a trend of increasing elastic moduli over time. The modulus for 7 DIV spheroids (160 ± 80 Pa) was twice that of 1 DIV spheroids (80 ± 30 Pa, $p < 0.05$), and 14 DIV spheroids (190 ± 70 Pa) and 21 DIV spheroids (240 ± 60 Pa) were 2.4- to 3-fold stiffer than 1 DIV spheroids ($p < 0.001$). The elastic modulus of neonatal cortex tissue (110 ± 70 Pa) was similar to the moduli of 1 DIV and 7 DIV spheroids, but lower than the moduli of 14 and 21 DIV spheroids ($p < 0.05$).

Discussion

In scaffold-free, self-assembled spheroid culture, cells form microtissues that contain a physiologically relevant microenvironment. In this study, we report a versatile and controllable 3D spheroid culture using postnatal, region-specific neural cells. These spheroids present many key features of the CNS microenvironment, including neuronal subtypes, glia, neural stem/progenitor cells, 3D structure, electrical activity, synapse formation, ECM protein production, and *in vivo*-like stiffness.

Versatile culture

The method we described herein provides several strengths. It uses commercially available materials, is cost-effective, and is reproducible in spheroid size and cellular composition. Specifically, it does not require lithography-based or other microelectronic approaches. It also avoids the variability associated with approaches such as hanging drop, spinner flask, and rotary systems.[21] Further, neither progenitor cell culture nor multistep differentiation is required here. This approach generates on the order of 1000 spheroids per neonate rat cortex, depending on the requisite spheroid cell density, thus demonstrating its potential for high-throughput assays and for reducing animal use. Spheroid sizes were controlled by initial seeding densities, with spheroids of all four seeding densities in this study reaching a stable size by 14 DIV. The spheroids in the micromolded hydrogels are easy to maintain, contain viable cells for at least 3 weeks, and are not allowed to fuse due to the micromold's physical barrier, thus providing researchers with a stable culture tool.

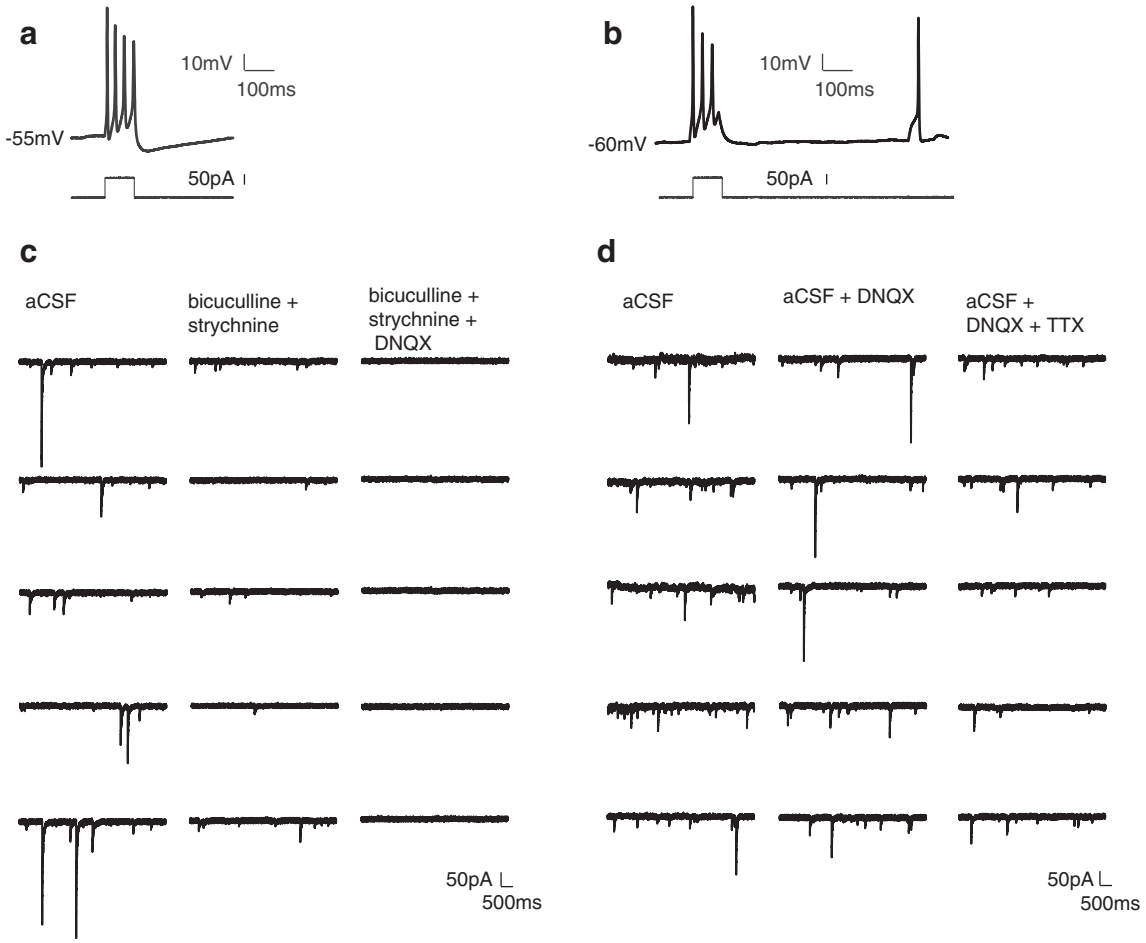

FIG. 4. Fourteen DIV spheroids contained mature neurons with synapses. Neurons in 14 DIV 8k spheroids fired both evoked and spontaneous action potentials. Both sEPSCs and sIPSCs were detected. **(a)** Evoked action potential. *Lower panel*: current injection step. **(b)** Example traces showing evoked action potentials followed by a spontaneous action potential. **(c)** *Left panel*: traces of spontaneous PSCs recorded in aCSF (voltage clamp recording at −70 mV). *Middle panel*: sEPSCs were isolated with $GABA_A$ receptor antagonist bicuculline and glycine receptor antagonist strychnine. *Right panel*: spontaneous PSCs were completely blocked with glutamate receptor antagonist DNQX, confirming that they were mediated by AMPA-type glutamate receptors. **(d)** *Left panel*: spontaneous PSCs recorded in aCSF (voltage clamp recording at −70 mV). *Middle panel*: sIPSCs were then isolated using DNQX. *Right panel*: traces of miniature sIPSCs remaining after addition of the sodium channel blocker tetradotoxin (TTX). These are individual quantal events.

This culture method has the potential to be applied to a wide range of neural cell types.[24] Here we have characterized rat postnatal cortical spheroids, and additionally, to demonstrate that other types of neural cells can self-assemble, we fabricated spheroids using rat hippocampal cells. Hippocampal cells from a commercially available tissue source formed spheroids, and the spheroid sizes were dependent on the seeding densities (Supplementary Fig. S5). We have previously fabricated spheroids from rat adult hippocampal neural stem cells and glioma cells.[24] This method also allows for coculture to study cell–cell interactions.[30] Of note, the seeding protocol allows for independent treatment of cell groups before combining them in the spheroid.[31]

In vivo-*like cell morphology and structure*

Cell density in the brain ($\sim 1 \times 10^5$ cells/mm^3 in mouse) is higher than in most other organs.[23,32] The spheroid culture allows for high density, which can mimic *in vivo* intercellular distance and communication better than scaffold cultures.[1] Cell density in spheroids at 1 DIV (2×10^6 cells/mm^3) was approximately one magnitude higher than *in vivo* density. Cell aggregation in the spheroid can be described as close packing of spheres,[33] thus the initial cell density within the spheroid is dependent on cell size rather than the number of cells per spheroid. Densities in the spheroids decreased as cells spread and extended processes over time, so that densities in 14–21 DIV spheroids ($2–4 \times 10^5$ cells/mm^3) approached the magnitude of *in vivo* density.

The 8k spheroids of this study provided microtissues that were easy to visualize and manipulate; however, after 21 DIV we observed the presence of centrally located pyknotic nuclei, as has been seen in other models.[9] We note that even in a microtissue containing some unhealthy cells, the healthy cells, including neurons, glia, and neural stem/progenitor cells, were able to extend robust networks of processes. Further, neurons in these spheroids were electrically active and formed synaptic connections. For future studies in which higher viability is required (e.g.,

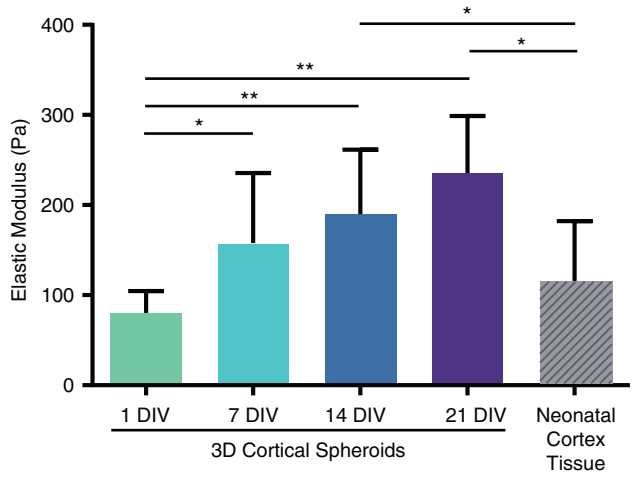

FIG. 5. Mechanical properties of 3D spheroids. Elastic moduli of 1, 7, 14, and 21 DIV 8k spheroids and of neonatal rat cortex tissues (P0-P2) were measured by atomic force microscope. There was a general trend of increasing elastic moduli over time in culture. Elastic moduli for 1 DIV and 7 DIV spheroids were not significantly different from those of neonatal rat cortex tissue while late-stage spheroids (14 and 21 DIV) had greater elastic moduli than neonatal rat cortex tissue. $*p < 0.05$, $**p < 0.001$. Color images available online at www.liebertpub.com/tec

models of hypoxia, injury, or stroke), smaller spheroids could be generated to optimize oxygen and nutrient diffusion.

Within the spheroids, neurites and cellular processes extended in all directions. Previous research showed that neurites in spheroids can extend to millimeters in length.[19] The period of increasing spheroid diameter correlated with the internal structural changes of growing extensions and increasing distance among nuclei.

Self-sorting of cell types has been seen in many heterotypic spheroid cultures.[34–36] In our cortical spheroids, glia were dispersed among the neurons, suggesting neuron–glia interactions, which are important *in vivo* for neuron homeostasis.[37] In future experiments, to approximate other cellular composition, such as that of adult brain, defined cell media could be used to promote proliferation of specific neural cells within the spheroid.

The importance of ECM has become increasingly recognized, especially since many neurological diseases are hallmarked by a change in the ECM composition.[38–40] In many scaffold-based cultures, the scaffold introduces foreign ECM to the microenvironment, which can potentially modify cell behavior and mask disease-related changes in the culture model. In the spheroids of this work, the cells produced all of the ECM. In the present study, we chose laminin as a candidate ECM molecule because of its role in neurogenesis, cell migration, axon guidance, oligodendrocyte maturation, and axon myelination.[41,42] Laminin production in the cortical spheroids demonstrated the culture's advantage of inherent production of ECM, as well as the absence of introduced foreign materials.

Active circuitry in the spheroid

Electrical activity and network formation through synapses are key functional features of neurons.[12,17,43–45] Whole-cell patch-clamp recording, used to assess electrophysiological properties of single neurons, has been difficult in 3D because scaffold materials break or occlude the ultrathin glass pipette tips. Thus, 3D cultures have typically been limited to extracellular field potential recordings of far lower resolution and generally do not identify neurotransmitter type.[1,16] Here, spheroids can be removed from the hydrogel mold and immobilized on coverslips, making this 3D culture compatible with patch-clamp recording. Whole-cell recordings at 14 and 21 DIV showed that the neurons in the spheroids had matured and were able to fire spontaneous and evoked action potentials associated with mature neurons. The difference in firing patterns among the neurons recorded may result from different neuronal subtypes within the spheroids. We note that resting membrane potentials of neurons in spheroids were less negative than *in vivo* (−64 mV).[46] One possible explanation is the greater synaptic connectivity in the spheroids. Spontaneous PSCs revealed functional synapse formation and robust communication among cells in the culture. Using specific pharmacological tools to block AMPA receptors and $GABA_A$ receptors, respectively, allowed us to characterize both excitatory and inhibitory synapses in the circuitry.

Brain-like mechanical properties

Neural cell functions such as differentiation, migration, neurite outgrowth, and response to toxins are affected by substrate stiffness.[2,7,47–49] In contrast to typical tissue culture materials—that is, polystyrene with an elastic modulus on the order of gigapascals—these cortical spheroids had elastic moduli in the range of neonatal brain tissue (110 Pa, this study) and of adult brain tissue (<1000 Pa).[50] The increase in spheroid elastic modulus over time correlated with changing cell morphology within the microtissues, as cells in spheroids were round when spheroids first self-assembled and spread in late-stage spheroids. These changes may reflect a previously demonstrated correlation between internal tension and actin bundle formation within spread cells.[27]

Although the commonly used cell culture hydrogels, collagen I gels (0.5–12 kPa)[51] and Matrigel (450 Pa),[52] also have elastic moduli in the range of brain tissue, they contain proteins that are not normally present in the brain. In the present study, spheroids contained only cell-secreted proteins. Taken together, spheroids' physiological mechanical properties may influence spheroid cellular behavior in beneficial ways.

Conclusions

Studies of the formation, health, pathology, and repair of the CNS have tremendous potential for advancement with the use of 3D *in vitro* approaches. Neurodegenerative disorders, brain injury, and neural connectivity are but a few of the issues demanding rigorous investigation. We have reported an efficient and effective method to culture primary cortical cells in 3D spheroids. Without replicating either the size or the organization of the cortex, we have generated a robust microtissue. The spheroids recapitulate several key features of the *in vivo* cortical tissue, including cell types, cell morphology, circuitry formation, ECM production, and mechanical properties. This 3D culture can serve as an attractive tool to study neurological disease and injury, to

screen therapeutic agents, and to gain insights into the organization and function of the CNS.

Acknowledgments

The authors thank William Sheeran for excellent technical assistance, and Geoffrey Williams of the Leduc Bioimaging Facility for excellent technical support with confocal microscopy. Funding was provided by NSF GK-12 Fellowship, Brown Institute for Brain Science Graduate Research Award, and the Department of Education through GAANN Award P200A090076 administered by the Institute for Molecular and Nanoscale Innovation at Brown University to Y.L.D.; NSF GRFP to M.E.B.; NIH NINDS SBIR 1R43NS073195 to J.R.M; NIH NIAMS R01AR063642 and NSF CBET 1253189 to E.M.D.; NIH NINDS R01NS088453 and NIH NIDA R01DA011289 to J.A.K.; NSF CBET 1134166, NIH 5R01HL110791 subcontract, NIH R21HL113918 subcontract, and Brown Institute for Brain Science Pilot Research Award to D.H.K.

Disclosure Statement

J.R.M. has an equity interest in MicroTissues, Inc. This relationship has been reviewed and managed by Brown University in accordance with its conflict of interest policies. No other competing financial interests exist.

References

1. Hopkins, A.M., DeSimone, E., Chwalek, K., and Kaplan, D.L. 3D in vitro modeling of the central nervous system. Prog Neurobiol **125,** 1, 2014.
2. Balgude, A.P., Yu, X., Szymanski, A., and Bellamkonda, R.V. Agarose gel stiffness determines rate of DRG neurite extension in 3D cultures. Biomaterials **22,** 1077, 2001.
3. Li, G.N., Livi, L.L., Gourd, C.M., Deweerd, E.S., and Hoffman-Kim, D. Genomic and morphological changes of neuroblastoma cells in response to three-dimensional matrices. Tissue Eng **13,** 1035, 2007.
4. Hoffman-Kim, D., Mitchel, J.A., and Bellamkonda, R.V. Topography, cell response, and nerve regeneration. Annu Rev Biomed Eng **12,** 203, 2010.
5. Bruder, J.M., Lee, A.P., and Hoffman-Kim, D. Biomimetic materials replicating Schwann cell topography enhance neuronal adhesion and neurite alignment in vitro. J Biomater Sci Polym Ed **18,** 967, 2007.
6. Baker, B.M., and Chen, C.S. Deconstructing the third dimension—how 3D culture microenvironments alter cellular cues. J Cell Sci **125,** 3015, 2012.
7. Georges, P.C., Miller, W.J., Meaney, D.F., Sawyer, E.S., and Janmey, P.A. Matrices with compliance comparable to that of brain tissue select neuronal over glial growth in mixed cortical cultures. Biophys J **90,** 3012, 2006.
8. Pampaloni, F., Reynaud, E.G., and Stelzer, E.H. The third dimension bridges the gap between cell culture and live tissue. Nat Rev Mol Cell Biol **8,** 839, 2007.
9. Lancaster, M.A., Renner, M., Martin, C.-A., Wenzel, D., Bicknell, L.S., Hurles, M.E., *et al.* Cerebral organoids model human brain development and microcephaly. Nature **501,** 373, 2013.
10. Choi, S.H., Kim, Y.H., Hebisch, M., Sliwinski, C., Lee, S., D'Avanzo, C., *et al.* A three-dimensional human neural cell culture model of Alzheimer's disease. Nature **515,** 274, 2014.
11. Cullen, D.K., Stabenfeldt, S.E., Simon, C.M., Tate, C.C., and LaPlaca, M.C. In vitro neural injury model for optimization of tissue-engineered constructs. J Neurosci Res **85,** 3642, 2007.
12. O'Shaughnessy, T.J., Lin, H.J., and Ma, W. Functional synapse formation among rat cortical neurons grown on three-dimensional collagen gels. Neurosci Lett **340,** 169, 2003.
13. Xu, T., Molnar, P., Gregory, C., Das, M., Boland, T., and Hickman, J.J. Electrophysiological characterization of embryonic hippocampal neurons cultured in a 3D collagen hydrogel. Biomaterials **30,** 4377, 2009.
14. Irons, H.R., Cullen, D.K., Shapiro, N.P., Lambert, N.A., Lee, R.H., and Laplaca, M.C. Three-dimensional neural constructs: a novel platform for neurophysiological investigation. J Neural Eng **5,** 333, 2008.
15. Frampton, J.P., Hynd, M.R., Shuler, M.L., and Shain, W. Fabrication and optimization of alginate hydrogel constructs for use in 3D neural cell culture. Biomed Mater **6,** 015002, 2011.
16. Odawara, A., Gotoh, M., and Suzuki, I. A three-dimensional neuronal culture technique that controls the direction of neurite elongation and the position of soma to mimic the layered structure of the brain. RSC Adv **3,** 23620, 2013.
17. Tang-Schomer, M.D., White, J.D., Tien, L.W., Schmitt, L.I., Valentin, T.M., Graziano, D.J., *et al.* Bioengineered functional brain-like cortical tissue. Proc Natl Acad Sci **111,** 13811, 2014.
18. Choi, Y.J., Park, J., and Lee, S.-H. Size-controllable networked neurospheres as a 3D neuronal tissue model for Alzheimer's disease studies. Biomaterials **34,** 2938, 2013.
19. Kato-Negishi, M., Morimoto, Y., Onoe, H., and Takeuchi, S. Millimeter-sized neural building blocks for 3D heterogeneous neural network assembly. Adv Healthc Mater **2,** 1564, 2013.
20. Fennema, E., Rivron, N., Rouwkema, J., van Blitterswijk, C., and de Boer, J. Spheroid culture as a tool for creating 3D complex tissues. Trends Biotechnol **31,** 108, 2013.
21. Lin, R.-Z., Lin, R.-Z., and Chang, H.-Y. Recent advances in three-dimensional multicellular spheroid culture for biomedical research. Biotechnol J **3,** 1172, 2008.
22. Puschmann, T.B., de Pablo, Y., Zandén, C., Liu, J., and Pekny, M. A novel method for three-dimensional culture of central nervous system neurons. Tissue Eng Part C Methods **20,** 485, 2014.
23. Pautot, S., Wyart, C., and Isacoff, E.Y. Colloid-guided assembly of oriented 3D neuronal networks. Nat Methods **5,** 735, 2008.
24. Boutin, M.E., and Hoffman-Kim, D. Application and assessment of optical clearing methods for imaging of tissue-engineered neural stem cell spheres. Tissue Eng Part C Methods **21,** 292, 2015.
25. Kuwajima, T., Sitko, A.A., Bhansali, P., Jurgens, C., Guido, W., and Mason, C. ClearT: a detergent- and solvent-free clearing method for neuronal and non-neuronal tissue. Development **140**, 1364, 2013.
26. Darling, E.M., Wilusz, R.E., Bolognesi, M.P., Zauscher, S., and Guilak, F. Spatial mapping of the biomechanical properties of the pericellular matrix of articular cartilage measured in situ via atomic force microscopy. Biophys J **98,** 2848, 2010.
27. Darling, E.M., Zauscher, S., Block, J.A., and Guilak, F. A thin-layer model for viscoelastic, stress-relaxation testing

of cells using atomic force microscopy: do cell properties reflect metastatic potential? Biophys J **92,** 1784, 2007.
28. Darling, E.M., Zauscher, S., and Guilak, F. Viscoelastic properties of zonal articular chondrocytes measured by atomic force microscopy. Osteoarthr Cartil **14,** 571, 2006.
29. Harding, J.W., and Sneddon, I.N. The elastic stresses produced by the indentation of the plane surface of a semi-infinite elastic solid by a rigid punch. Math Proc Cambridge Philos Soc **41,** 16, 1945.
30. Achilli, T., McCalla, S., Tripathi, A., and Morgan, J.R. Quantification of the kinetics and extent of self-sorting in three dimensional spheroids. Tissue Eng Part C Methods **18,** 302, 2012.
31. Youssef, J., Chen, P., Shenoy, V.B., and Morgan, J.R. Mechanotransduction is enhanced by the synergistic action of heterotypic cell interactions and TGF-1. FASEB J **26,** 2522, 2012.
32. Herculano-Houzel, S., and Lent, R. Isotropic fractionator: a simple, rapid method for the quantification of total cell and neuron numbers in the brain. J Neurosci **25,** 2518, 2005.
33. Curcio, E., Salerno, S., Barbieri, G., De Bartolo, L., Drioli, E., and Bader, A. Mass transfer and metabolic reactions in hepatocyte spheroids cultured in rotating wall gas-permeable membrane system. Biomaterials **28,** 5487, 2007.
34. Napolitano, A.P., Dean, D.M., Man, A.J., Youssef, J., Ho, D.N., Rago, A.P., *et al.* Scaffold-free three-dimensional cell culture utilizing micromolded nonadhesive hydrogels. Biotechniques **43,** 494, 2007.
35. Rago, A.P., Dean, D.M., and Morgan, J.R. Controlling cell position in complex heterotypic 3D microtissues by tissue fusion. Biotechnol Bioeng **102,** 1231, 2009.
36. Dean, D.M., and Morgan, J.R. Cytoskeletal-mediated tension modulates the directed self-assembly of microtissues. Tissue Eng Part A **14,** 1989, 2008.
37. Allen, N.J., and Barres, B.A. Neuroscience: glia—more than just brain glue. Nature **457,** 675, 2009.
38. Lau, L.W., Cua, R., Keough, M.B., Haylock-Jacobs, S., and Yong, V.W. Pathophysiology of the brain extracellular matrix: a new target for remyelination. Nat Rev Neurosci **14,** 722, 2013.
39. Morgan, C., and Inestrosa, N.C. Interactions of laminin with the amyloid beta peptide. Implications for Alzheimer's disease. Braz J Med Biol Res **34,** 597, 2001.
40. Liesi, P., Kaakkola, S., Dahl, D., and Vaheri, A. Laminin is induced in astrocytes of adult brain by injury. EMBO J **3,** 683, 1984.
41. Relucio, J., Menezes, M.J., Miyagoe-Suzuki, Y., Takeda, S., and Colognato, H. Laminin regulates postnatal oligodendrocyte production by promoting oligodendrocyte progenitor survival in the subventricular zone. Glia **60,** 1451, 2012.
42. Barros, C.S., Franco, S.J., and Müller, U. Extracellular matrix: functions in the nervous system. Cold Spring Harb Perspect Biol **3,** 1, 2011.
43. Dichter, M.A. Rat cortical neurons in cell culture: culture methods, cell morphology, electrophysiology, and synapse formation. Brain Res **149,** 279, 1978.
44. Zhang, Y., Pak, C., Han, Y., Ahlenius, H., Zhang, Z., Chanda, S., *et al.* Rapid single-step induction of functional neurons from human pluripotent stem cells. Neuron **78,** 785, 2013.
45. Frega, M., Tedesco, M., Massobrio, P., Pesce, M., and Martinoia, S. Network dynamics of 3D engineered neuronal cultures: a new experimental model for in-vitro electrophysiology. Sci Rep **4,** 5489, 2014.
46. Jia, H., Rochefort, N.L., Chen, X., and Konnerth, A. Dendritic organization of sensory input to cortical neurons in vivo. Nature **464,** 1307, 2010.
47. Ramamoorthi, K., Hara, J., Ito, C., and Asuri, P. Role of three-dimensional matrix stiffness in regulating the response of human neural cells to toxins. Cell Mol Bioeng **7,** 278, 2014.
48. Man, A.J., Davis, H.E., Itoh, A., Leach, J.K., and Bannerman, P. Neurite outgrowth in fibrin gels is regulated by substrate stiffness. Tissue Eng Part A **17,** 2931, 2011.
49. Saha, K., Keung, A.J., Irwin, E.F., Li, Y., Little, L., Schaffer, D. V., *et al.* Substrate modulus directs neural stem cell behavior. Biophys J **95,** 4426, 2008.
50. Elkin, B.S., Azeloglu, E.U., Costa, K.D., and Morrison, B. Mechanical heterogeneity of the rat hippocampus measured by atomic force microscope indentation. J Neurotrauma **24,** 812, 2007.
51. Raub, C.B., Putnam, A.J., Tromberg, B.J., and George, S.C. Predicting bulk mechanical properties of cellularized collagen gels using multiphoton microscopy. Acta Biomater **6,** 4657, 2010.
52. Soofi, S.S., Last, J.A., Liliensiek, S.J., Nealey, P.F., and Murphy, C.J. The elastic modulus of Matrigel™ as determined by atomic force microscopy. J Struct Biol **167,** 216, 2009.

Address correspondence to:
Diane Hoffman-Kim, PhD
Department of Molecular Pharmacology, Physiology and Biotechnology
Brown University
Box G-B
Providence, RI 02912

E-mail: diane_hoffman-kim@brown.edu

Received: March 19, 2015
Accepted: August 27, 2015
Online Publication Date: October 6, 2015